mater.scichina.com link.springer.com

Published online 28 December 2020 | https://doi.org/10.1007/s40843-020-1536-6
Sci China Mater 2021, 64(6): 1408–1417

Three-dimensional hierarchical Co(OH)F nanosheet arrays decorated by single-atom Ru for boosting oxygen evolution reaction

Shizheng Zhou[1†], Haeseong Jang[2†], Qing Qin[1*], Zijian Li[3], Min Gyu Kim[4], Chuang Li[1], Xien Liu[1*] and Jaephil Cho[2*]

ABSTRACT **Electronic coupling with the support plays a crucial role in boosting the intrinsic catalytic activity of a single-atom catalyst. Herein, the three-dimensional (3D) hierarchical Co(OH)F nanosheet arrays modified by single-atom Ru (SA-Ru/Co(OH)F) are prepared by a facile one-step hydrothermal method under mild conditions, which exhibit excellent activity with an overpotential of 200 and 326 mV at 10 and 500 mA cm^{-2}, respectively, as well as robust stability for oxygen evolution reaction (OER) in 1.0 mol L^{-1} KOH electrolyte. The study of electronic structures and surface chemical states before and after OER testing reveals that the strong electronic coupling between single-atom Ru and Co(OH)F induces the charge redistribution in SA-Ru/Co(OH)F and suppresses the excessive oxidation of Ru into higher valence state (more than +4) under high OER potential. This work provides a strategy to stabilize single-atom Ru by Co(OH)F that can enhance the activity and durability for OER under large current densities.**

Keywords: electrocatalyst, oxygen evolution reaction, single atom, ruthenium, electronic coupling

INTRODUCTION

Producing clean and sustainable hydrogen by water electrolysis is considered as the most promising way to relieve the increasing energy and environmental pressures [1–3]. However, as one of the half reaction occurring at the anode, the oxygen evolution reaction (OER) severely limits the energy conversion efficiency due to the complex four-electron transfer process and thus leads to sluggish kinetics [4–6]. A highly effective electrocatalyst is indispensable to reduce the reaction barrier and enhance the rate of OER [7]. To meet the requirement of industrial water electrolysis in alkaline electrolyte, the efficient OER electrocatalyst should be durable at large current densities of more than 200 mA cm^{-2} [8]. Currently, noble metal-based catalysts, such as IrO_2 and RuO_2, are the state-of-the-art OER electrocatalysts, but the low earth abundance and exorbitant price impede their further commercialization [9]. Moreover, the stability of RuO_2 for long-term electrocatalysis easily becomes poor because of RuO_4^{2-} formed in alkaline electrolyte after OER testing [10–12]. Therefore, to develop cost-effective, active, and durable alternatives to noble-based catalysts as the OER electrocatalyst still remains a big challenge.

Single-atom catalysts have recently received extensive research interests due to the unique electronic properties and effective atom utilization [13,14]. Due to the thermodynamical unstability and the trend to aggregate [15], effective support is absolutely indispensable to stabilize the single atoms. Common monoatomic supports include carbon materials [16], metal-organic frameworks, metal oxide, boron nitride, and layered double hydroxides (LDHs) [17]. The catalytic activity of single-atom catalyst is largely affected by the local coordination environments through the electronic and geometric interaction between

[1] State Key Laboratory Base of Eco-Chemical Engineering, College of Chemical Engineering, Qingdao University of Science and Technology, Qingdao 266042, China
[2] Department of Energy Engineering, Department of Energy and Chemical Engineering, Ulsan National Institute of Science and Technology (UNIST), Ulsan 44919, South Korea
[3] Department of Chemistry, City University of Hong Kong, Hong Kong, China
[4] Beamline Research Division, Pohang Accelerator Laboratory (PAL), Pohang 37673, South Korea
[†] These authors contributed equally to this work.
[*] Corresponding authors (emails: qinqing@qust.edu.cn (Qin Q); liuxien@qust.edu.cn (Liu X); jpcho@unist.ac.kr (Cho J))

the support and single atoms [18]. Due to the potential charge transfer between single atoms and the support, the charge redistribution leads to varied charge density, which would affect the catalytic activity of single-atom catalysts [19]. As reported, the $Ti_3C_2O_2$-supported single Pd atom exhibited a low overpotential of 310 mV to deliver 10 mA cm^{-2}, attributable to optimal d band center of the supported Pd [20]. Thus, the intrinsic catalytic activity of single-atom active sites could be boosted *via* anchoring them on appropriate supports.

Recently, Co(OH)F has been considered as an effective support for noble metal catalysts due to their exceptional electronic configurations [21], abundant base active sites [17] and special channel structure [22]. As reported by a previous study, Co(OH)F-supported PtO_2 exhibited enhanced activity for hydrogen evolution reaction (HER) in alkaline electrolyte attributable to the synergetic interface effect between two moieties. Apart from serving as the support, the Co(OH)F can also act as active species for catalyzing electrode reaction. For instance, three-dimensional (3D) Co(OH)F microspheres exhibited an overpotential of 313 mV for the OER to deliver the current density of 10 mA cm^{-2} [23]. The carbon fiber paper-supported ultralong needle-like N-doped Co(OH)F could achieve the OER current density of 10 mA cm^{-2} at a potential of 1.54 V (*vs.* reversible hydrogen electrode (RHE)) in 1.0 mol L^{-1} KOH [24]. To achieve large catalytic current density as well as avoid the aggregation of Co-based materials resulting from the strong magnetism [21], *in-situ* growth of catalyst nanoarrays on conductive substrates would be a promising and facile approach [25]. Constructing 3D cross nanosheet arrays could provide the potential of combining numerous merits into a single structure: short diffusion distance for electrolyte ions and electrons, as well as large surface-to-volume ratio in stark contrast to bulk counterparts; large open spaces could afford more accessible active sites and favorable mass diffusion [26]; interconnectivity of nanosheets is conducive to charge transport within the framework [27]. There is no need using polymer binder to hold the catalyst, which is beneficial for reducing dead volume, further contributing to exposed active atom sites [28]. Avoiding the peeling of catalytic active species during the OER process is also a non-negligible problem for long-term maintaining stability at large current densities.

Herein, we report 3D hierarchical Co(OH)F nanosheet arrays modified by single-atom Ru (SA-Ru/Co(OH)F), which exhibits outstanding OER activity and stability in 1.0 mol L^{-1} KOH solution. The *ex-situ* X-ray photoelectron spectroscopy (XPS) and X-ray absorption near edge structure (XANES) reveal that the existence of strong electronic coupling between SA-Ru and Co(OH)F support inhibits the over-oxidation of Ru at even high applied potential, which, together with advantages of 3D array structure, renders the SA-Ru/Co(OH)F superior OER activity and stability than RuO_2 and most of the reported catalysts. For overall water splitting, the assembled SA-Ru/Co(OH)F||Pt/C cell only needs a voltage of 1.56 V to achieve a current density of 10 mA cm^{-2}, which is 80 mV lower than that of RuO_2-Pt/C pairs. This work provides a strategy for improving the OER performance of non-noble metal-based electrocatalysts.

EXPERIMENTAL SECTION

Chemicals

$RuCl_3{\cdot}xH_2O$ (molecular weight: 207.43), NH_4F, urea and $Co(NO_3)_2{\cdot}6H_2O$ were purchased from J&K Scientific Ltd. The other reagents were purchased and directly used without further purification.

Syntheses of SA-Ru/Co(OH)F and Co(OH)F nanosheet arrays

In a typical procedure, 5 mmol of urea and 4 mmol of NH_4F were added into 12 mL of deionized (DI) water and the solution was stirred for 10 min. Then, 0.909 mmol of $Co(NO_3)_2{\cdot}6H_2O$ was added into the solution. After stirring for another 10 min, $RuCl_3{\cdot}xH_2O$ (0.0476 mmol, corresponding to Ru/(Ru+Co) = 5%) was added, and the resultant homogenous solution was transferred into a 20-mL stainless-steel autoclave, in which a piece of pretreated Ni foam (1 cm × 1.5 cm) was put in advance. The autoclave was then heated to 100°C. After reaction for 8 h, the autoclave was cooled to room temperature naturally. The Ni foam coated with catalysts was taken out and gently washed with DI water, and finally vacuum-dried at 60°C for 2 h. The same synthetic process was adopted to prepare the Ru/Co(OH)F with different Ru contents (Ru/(Ru+Co) = 2%, 10%) by varying the dosage of $RuCl_3{\cdot}xH_2O$.

The synthetic method of Co(OH)F nanosheet array is similar with that of SA-Ru/Co(OH)F nanosheet array, but without adding $RuCl_3{\cdot}xH_2O$ at the initial process.

Electrochemical measurements

Oxygen evolution reaction

The OER performance of all the prepared catalysts was evaluated in a typical three-electrode configuration with a carbon rod as the counter electrode and a Hg/HgO

electrode selected as the reference electrode, respectively. The Ni foam (0.5 cm × 1.0 cm) coated with catalyst by *in-situ* growth was directly used as the working electrode (catalyst loading amount: ~3.5 mg cm^{-2}). The 1.0 mol L^{-1} KOH was used as the electrolyte. All potentials were obtained by using the RHE as the reference. The polarization curves were measured at a scan rate of 5 mV s^{-1} in the potential range of 1.0–2.0 V (*vs.* RHE). All the data were obtained with 95% *iR* (the voltage loss caused by ohmic resistance) compensation. Electrochemical impedance spectroscopy (EIS) was carried out under an amplitude of 5 mV at an open circuit voltage with a range of 100 kHz–0.1 Hz. The durability testing was carried out using the chronoamperometry method at potentials of 1.43, 1.52 and 1.56 V (*vs.* RHE), respectively, for 80,000 s. The double-layer capacitance (C_{dl}) was used to evaluate the electrochemical active surface area (ECSA) of the materials, which was measured in a non-Faradaic potential window from 1.17 to 1.29 V (*vs.* RHE) with varied scan rates from 20 to 120 mV s^{-1}.

Overall water splitting

The overall water splitting performance of the prepared SA-Ru/Co(OH)F as the anode was investigated in a two-electrode cell with commercial Pt/C (20 wt%) as the cathode. For comparison, the performance of overall water splitting cells assembled with commercial RuO_2-Pt/C pairs was also recorded at the same conditions. The 1.0 mol L^{-1} KOH solution was used as electrolyte. The testing voltage ranges from 0.9 to 2.2 V. The polarization curves were measured at a scan rate of 5 mV s^{-1}. The electrochemical stability testing was conducted at a constant voltage of 1.56 V for 70,000 s.

RESULTS AND DISCUSSION

SA-Ru/Co(OH)F nanoarrays were *in-situ* grown on Ni foam *via* a simple hydrothermal route at a relatively low temperature. After getting rid of Ni foam, the resultant samples were tested for physical characterization. Scanning electron microscopy (SEM) images in Fig. 1a and Fig. S1 show a 3D network architecture characterized by

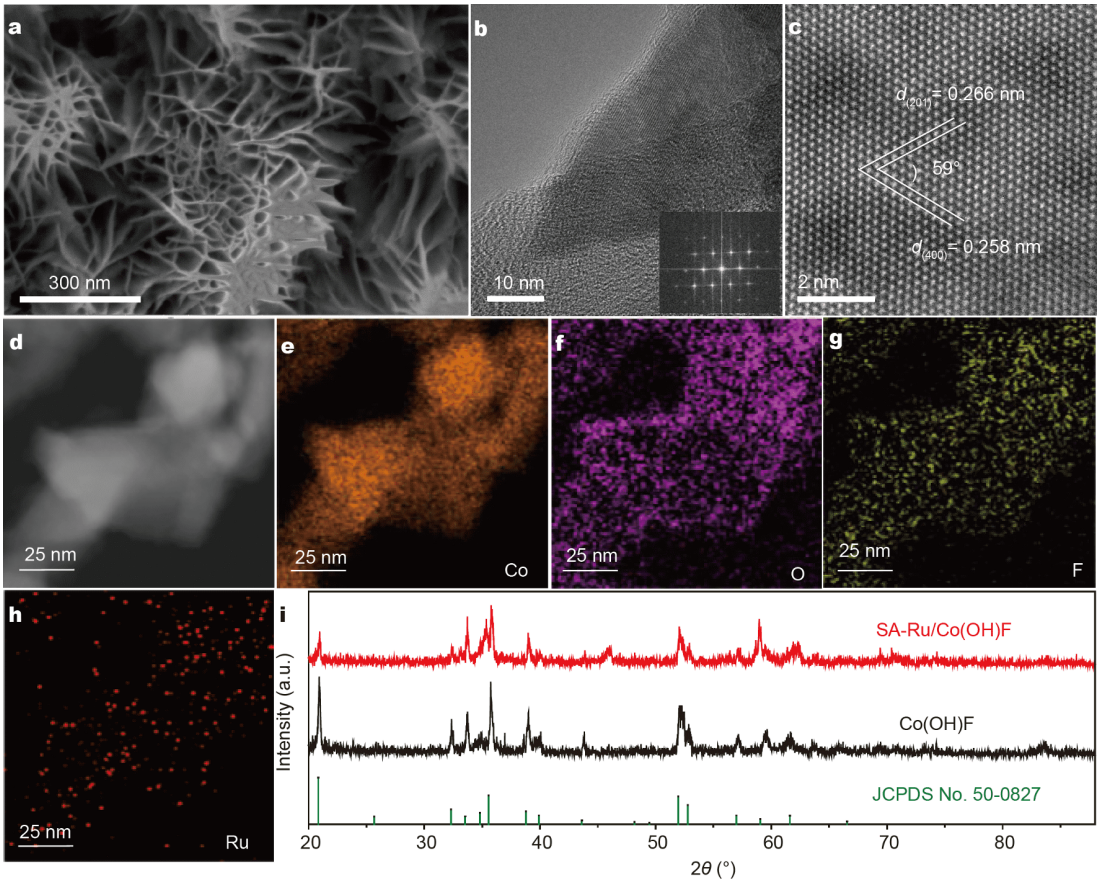

Figure 1 Characterizations of the as-synthesized SA-Ru/Co(OH)F nanoarrays: (a) SEM image; (b) TEM image (inset shows the FFT pattern); (c) ADF-STEM image; (d–h) HAADF-STEM image and corresponding elemental mappings of Co, O, F and Ru; (i) XRD patterns of Co(OH)F and SA-Ru/Co(OH)F.

hierarchical nanosheet arrays that endows the SA-Ru/Co(OH)F with a large specific surface area. The 3D network architecture provides more exposed active sites and favors the contact of electrode materials with electrolyte, as well as benefits the diffusion of reactants and release of produced gas in numerous 3D cavities; all these advantages greatly contribute to improving the activity and reaction kinetics of OER [29,30]. Fig. 1b shows the typical transmission electron microscopy (TEM) image of an SA-Ru/Co(OH)F nanosheet, which exhibits the lattice fringe corresponding to bare Co(OH)F, and the inset displays the fast Fourier transform (FFT) pattern, demonstrating the single-crystal nature of the Co(OH)F nanosheet with an orthorhombic structure. No apparent metallic ruthenium particles or clusters can be observed, and the atomically dispersed Ru is demonstrated by the following XANES and extended X-ray absorption fine structure (EXAFS) spectra. In the annular dark field scanning TEM (ADF-STEM) image (Fig. 1c), the lattice spacings of 0.258 and 0.266 nm are easily indexed to (400) and (201) planes of Co(OH)F. The intersection angle between the two facets is measured about 59°, which is consistent with the value that calculated according to the dihedral angle formula of orthorhombic crystal structure [23]. A high-angle annular dark field STEM (HAADF-STEM) image and the corresponding energy-dispersive X-ray (EDX) elemental mapping images are shown in Fig. 1d–h, further demonstrating the composition of the prepared catalyst and the homogeneous anchoring of Ru on the Co(OH)F. Fig. 1i shows the X-ray diffraction (XRD) pattern of SA-Ru/Co(OH)F is similar to that of the bare Co(OH)F, which possesses an orthorhombic structure with unit cell parameters of a = 10.305 Å, b = 4.677 Å, and c = 3.126 Å (JCPDS No. 50-0827). The impurity peak at 45.6° belongs to the Ni foam [31]. No diffraction peaks can be assigned to Ru species because of its ultra-low content of 0.5 wt% analyzed by inductively coupled plasma atom emission spectrometry (ICP-AES) analysis.

To gain insights into the surface chemical states of SA-Ru/Co(OH)F and the changes of surface electronic structures before and after OER testing, the XPS, XANES, and EXAFS measurements were performed. Four fundamental elements including Ru, Co, O and F can be found in the XPS survey spectrum (Fig. S2), further confirming the elemental composition of the prepared SA-Ru/Co(OH)F. Fig. 2a shows the high-resolution XPS spectra of Ru 3p for SA-Ru/Co(OH)F before and after OER testing. Before testing, the Ru 3p spectrum is deconvoluted into two peaks with binding energies of 485.6 and 463.9 eV, lower than that of Ru^{4+} state [32,33]. The negative core-level shift of Ru compared with that of Ru(IV) in RuO_2 reveals the high electronic density of Ru sites in SA-Ru/Co(OH)F system [34], which results from the charge transfer from Co to Ru by bridging O due to the relatively large electronegativity of Ru (2.2) than Co (1.88) [11,35]. After OER testing, a positive shift by 0.2 eV is observed for Ru 3p spectrum of SA-Ru/Co(OH)F-A (A represents the catalyst collected after OER testing), which is attributed to the slight electron transfer from Ru to the adsorbed OER oxygen-containing intermediates. Even so, the valence state of monatomic Ru is still lower than +4, indicating no overoxidation of Ru to unstable phase ($Ru^{(4+\delta)+}$, $\delta > 0$), which will be easy to dissolve and thus lead to degradation of catalyst performance [36]. In the Co $2p_{3/2}$ spectrum of Co(OH)F, two peaks located approximately at 780.9 and 783.0 eV, while a broad satellite peak located at 786.5 eV, are observed (Fig. 2b). The positions of these peaks are in accordance with Co $2p_{3/2}$ signal from Co^{II} species with unpaired 3d electrons, as reported by the previous studies [23,37]. When the Ru single atom anchored on Co(OH)F, the main peak (780.9 eV) of Co $2p_{3/2}$ spectrum of SA-Ru/Co(OH)F slightly shifts to a lower binding energy of 780.6 eV, close to the position of Co^{3+} (780.4 eV) [37], indicating the charge transfer from Co to Ru element due to the larger electronegativity of Ru than Co. The further negative shift in the binding energies occurring for SA-Ru/Co(OH)F after OER testing may arise from the oxidation of Co during the catalysis [38]. The F 1s spectrum of Co(OH)F is shown in Fig. S3a, which displays a single peak at 684.2 eV matching well with the position of F^- in metal hydroxyfluoride [39]. The peak of F 1s spectrum exhibits a slight right-shift of 0.3 eV for SA-Ru/Co(OH)F. This may be attributed to the increase in charge density of the whole catalyst after introduction of Ru and the large electronegativity of F element. After OER testing, the binding energy of F 1s of SA-Ru/Co(OH)F-A is more negative and the value is observed as 683.8 eV. As shown in Fig. S3b, the fitted main peak of O 1s spectrum for Co(OH)F is at a binding energy of 531.4 eV, similar to that of OH^- in metal hydroxides. A smaller peak centered at 532.7 eV can be assigned to the chemisorbed water molecules [40]. A new peak appearing at 530.1 eV belongs to the Ru–O bonds due to the formation of Ru–O–Co bond when SA-Ru is anchored on Co(OH)F. All those peaks of O 1s spectrum shift to low energy side to accommodate electrons when Ru is introduced to the Co(OH)F system, because the O acts as a bridge for electron transport between Ru and Co. After OER testing, the three peaks corresponding to H_2O (or OOH), OH^-,

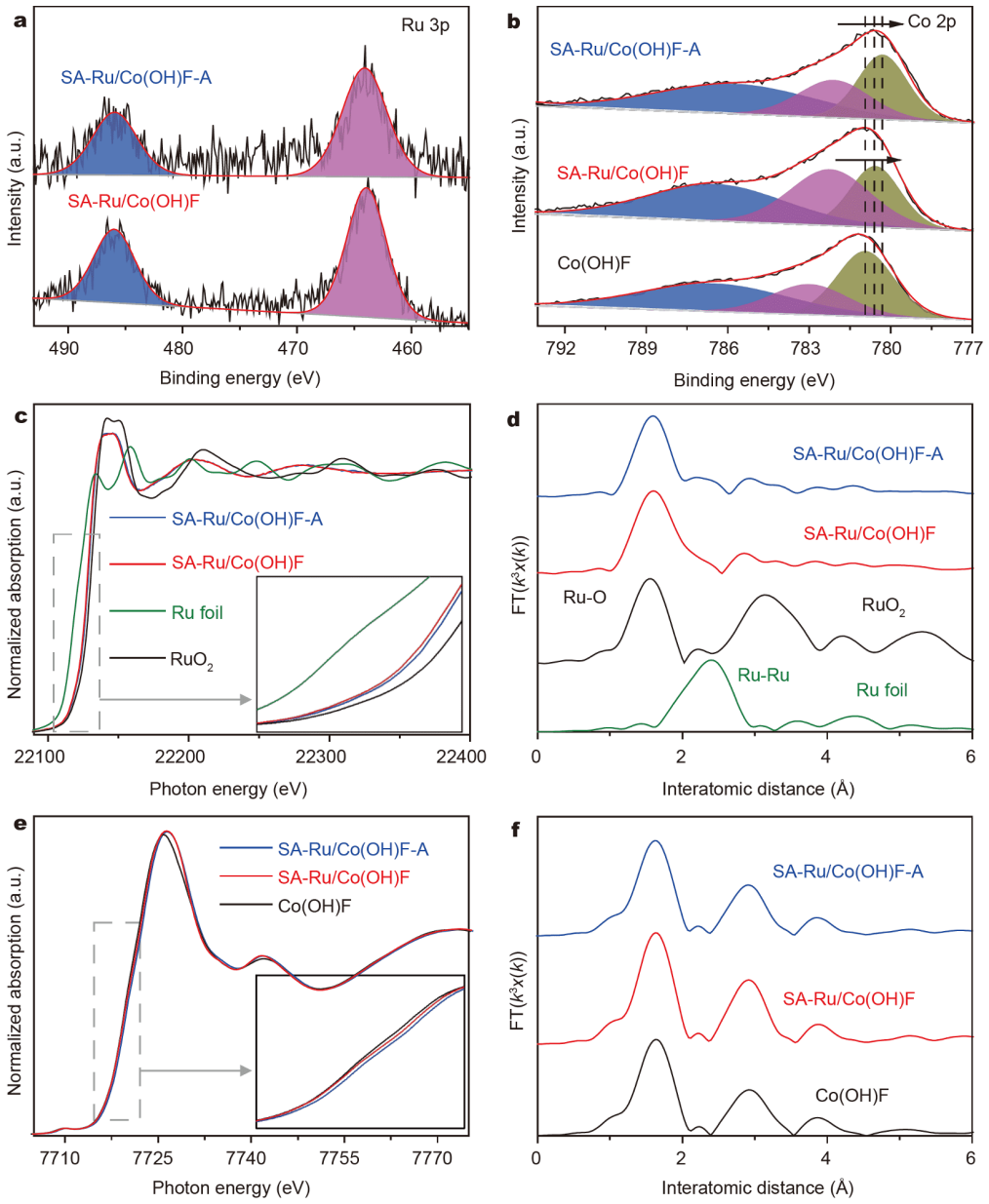

Figure 2 XPS spectra of (a) Ru 3p and (b) Co 2p of SA-Ru/Co(OH)F before and after OER testing. (c) Ru K-edge XANES spectra and (d) Fourier transforms of the Ru K-edge EXAFS spectra of Ru foil, RuO_2, SA-Ru/Co(OH)F and SA-Ru/Co(OH)F-A. (e) Co K-edge XANES spectra and (d) Fourier transforms of the Co K-edge EXAFS spectra of Co(OH)F, SA-Ru/Co(OH)F and SA-Ru/Co(OH)F-A.

and O^{2-} (bonded with Co) negatively shift to 532.0, 530.8 and 529.0 eV, respectively, due to the donation of electrons by adsorbed OH.

Fig. 2c shows the XANES spectra of SA-Ru/Co(OH)F, SA-Ru/Co(OH)F-A, as well as Ru foil and commercial RuO_2 for comparison. Evidently, the adsorption edge of SA-Ru/Co(OH)F is positioned between RuO_2 and Ru foil, implying that the average valence of Ru in the SA-Ru/Co(OH)F is between +4 and 0 [11,41]. Moreover, the adsorption edge of Ru in SA-Ru/Co(OH)F-A slightly shifts to high energy, demonstrating the increase of Ru valence state after OER testing. These agree well with the XPS analysis results. The corresponding Fourier transformed EXAFS (FT-EXAFS) spectra of Ru K-edge for the above four samples are shown in Fig. 2d. For the curve of SA-Ru/Co(OH)F, a main peak appearing at 1.61 Å results

from the Ru–O bonds, which is elongated compared with that of RuO_2 (1.55 Å). The weak peak at 2.84 Å corresponds to Ru–O–Co bonds [17]. No peaks assigned to Ru–Ru bonds (2.41 Å) are observed, effectively indicating that Ru exists in a form of single atom [42]. After OER testing, the Ru–O peak negatively shifts to 1.58 Å but is still stronger than that of RuO_2, implying that Ru oxidation state is lower than +4. This result avoids the further oxidation of Ru to high valence state (> +4) that can easily migrate into the electrolyte. The XANES spectra of Co K-edge of bare Co(OH)F, SA-Ru/Co(OH)F, and SA-Ru/Co(OH)F-A are displayed in Fig. 2e. The Co K-edge XANES of SA-Ru/Co(OH)F exhibits a more positive energy compared with Co(OH)F, but lower than CoOOH [43], indicating the oxidation state of Co in SA-Ru/Co(OH)F is between +2 and +3. After OER testing, the absorption peak of SA-Ru/Co(OH)F-A further evidently right-shifts to 7726.6 eV, much close to that of CoOOH, demonstrating the oxidation of initial Co^{2+} to a higher state during the OER process [44]. As depicted in Fig. 2f, the EXAFS spectra of Co K-edge show the shortened bond length (1.634 Å) of the nearest shell of SA-Ru/Co(OH)F compared with that of bare Co(OH)F (1.641 Å), which is closely related to the increased oxidation of Co ions [43,45,46]. Because the Co^{2+} is oxidized to close to Co^{3+} during the oxygen evolution, the bond length for the first coordination shell of SA-Ru/Co(OH)F-A is further contracted to 1.628 Å. The shortening in bonds is beneficial to further fixing the Ru atom, thereby stabilizing the single-atom Ru and avoiding possible dissolution when the oxidation state changes [17].

The electrocatalytic performance of the as-synthesized SA-Ru/Co(OH)F and references supported on Ni foam toward OER was systematically studied in a conventional three-electrode setup in 1.0 mol L^{-1} KOH solution. As shown in Fig. 3a, the iR-compensated OER polarization curves were used to evaluate the activities of OER. As known, the current densities of industrial water electrolysis in alkaline solution are approximately 200–400 mA cm^{-2}, and metal or alloy Ni are commonly used electrode materials; therefore, we also compared the activities of the catalyst and references at large current densities, such as 500 mA cm^{-2}. The SA-Ru/Co(OH)F exhibits an outstanding OER activity, characterized by the lower overpotentials of 200, 289, and 326 mV corresponding to different current densities of 10, 100, and 500 mA cm^{-2}, respectively, which are obviously lower than those of Co(OH)F (319, 374, and 460 mV) and bench mark RuO_2 (332, 400, and 526 mV) at the same current densities (Fig. 3b). Fig. 3c shows the Tafel plots derived from the polarization curves in Fig. 3a. The SA-Ru/Co(OH)F owns the favorable OER kinetics with a smaller Tafel slope of 76 mV dec^{-1}, much smaller than those of Co(OH)F (86 mV dec^{-1}), Ni foam (90 mV dec^{-1}), and RuO_2 (82 mV dec^{-1}). Noteworthily, the SA-Ru/Co(OH)F displays competitive OER activity compared with the recently reported efficient catalysts in alkaline environment (Fig. 3g and Table S1). To realize the industrialization of alkaline water electrolysis, oxygen evolution at high current density is a fundamental requirement [47]. Therefore, the durabilities of SA-Ru/Co(OH)F at constant overpotentials of 200, 289, and 326 mV were all measured. As illustrated in Fig. 3d, the SA-Ru/Co(OH)F shows excellent stability at various potentials for continuous water oxidation for 80,000 s. Especially, the activity of catalyst is obviously improved after *i-t* stability testing at a large current density. The XRD patterns of SA-Ru/Co(OH)F show the composition and structure undergo negligible changes after stability testing (Fig. S4). The Nyquist plots derived from the EIS show that the charge-transfer resistance (R_{ct}) of SA-Ru/Co(OH)F is obviously lower than that of Co(OH)F (Fig. 3e), demonstrating that the introduction of Ru enables the faster electron transfer as well as catalytic reaction kinetics [48]. The Brunauer-Emmett-Teller (BET) specific surface area of SA-Ru/Co(OH)F is determined to be 5.73 $m^2 g^{-1}$ by N_2 adsorption-desorption curves (Fig. S5). The smaller specific surface area suggests that the highly catalytic activity of SA-Ru/Co(OH)F is mainly related to its highly intrinsic catalytic activity. The electrochemical C_{dl} is proportional to the ECSA [49,50], which can be calculated from the non-Faradaic region, as shown in Fig. S6. As a result, Fig. 3f shows the C_{dl} of SA-Ru/Co(OH)F is 54.1 mF cm^{-2}, which is more than three times that of Co(OH)F (17.6 mF cm^{-2}), indicating that the incorporation of Ru single atom into Co(OH)F nanostructure could create more active sites. The general specific capacitance (C_s) of 0.04 mF cm^{-2} was applied to calculate the ECSA value [51]. The ECSA values are 676.25 and 220.0 for SA-Ru/Co(OH)F and Co(OH)F, respectively. The ECSA normalized linear scan voltammogram (LSV) curves of SA-Ru/Co(OH)F and Co(OH)F are displayed in Fig. S7. According to the previous studies, single-atom Ru dispersed on CoFe LDHs could effectively tune the electronic structure of Ru and optimal adsorption free energy of the rate-determining step (forming *OOH) [17], and thus lead to the enhanced intrinsic catalytic activity. The loading of Ru is a key factor that greatly influences the OER catalytic performance of Ru/Co(OH)F. Thus, a series of Ru dosage-

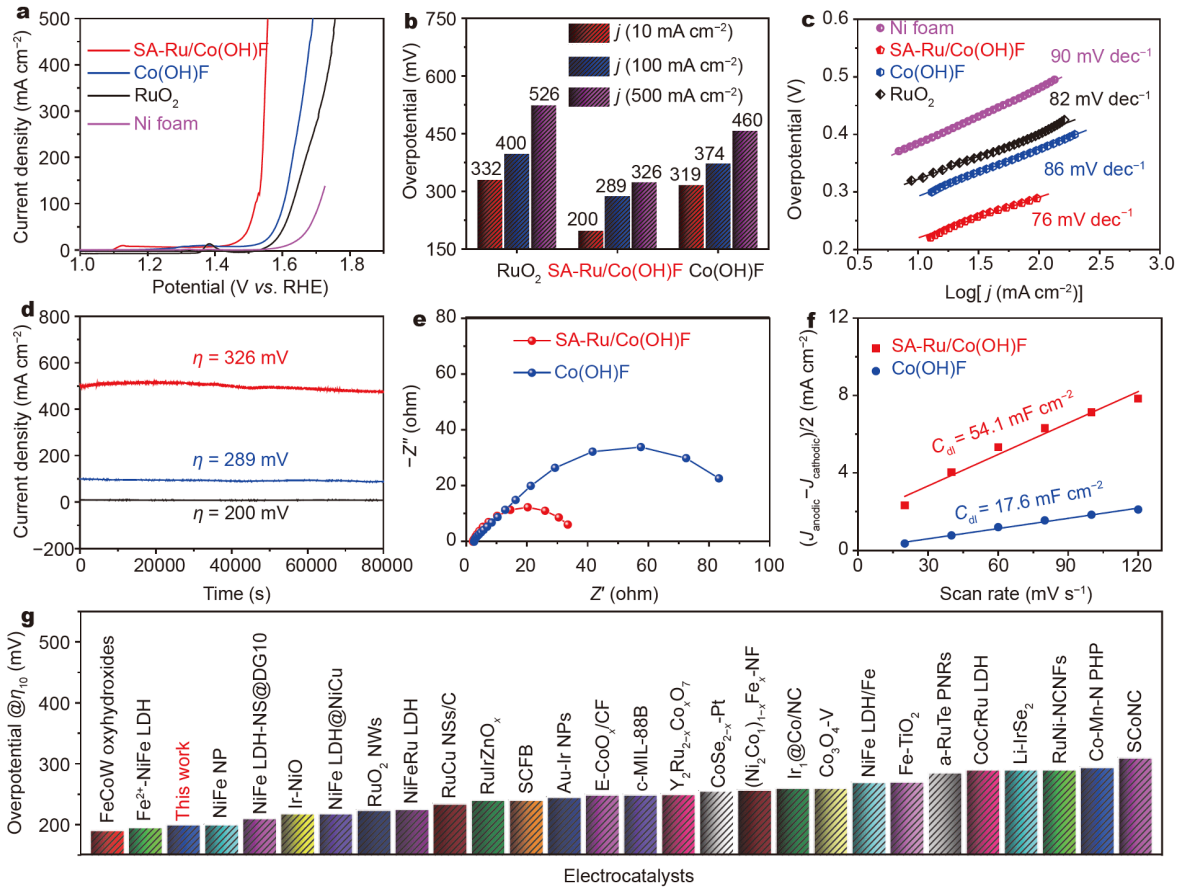

Figure 3 (a) LSV curves of SA-Ru/Co(OH)F, Co(OH)F, commercial RuO_2 and Ni foam in 1.0 mol L^{-1} KOH electrolyte. (b) Overpotentials for different current densities. (c) Tafel slopes of SA-Ru/Co(OH)F, Co(OH)F, RuO_2 and Ni foam. (d) Time-dependent current densities of SA-Ru/Co(OH)F. (e) Nyquist plots for SA-Ru/Co(OH)F and Co(OH)F measured at open-circuit voltage. (f) Capacitive $\Delta j/2$ (j: the current measured in non-Faradaic potential region) as a function of the scan rate for SA-Ru/Co(OH)F and Co(OH)F. (g) Comparison of overpotential of SA-Ru/Co(OH)F at j = 10 mA cm^{-2} with other reported catalysts (see details in Table S1).

dependent experiments were conducted by changing the amount of Ru raw material from the mass ratio of Ru/(Ru +Co) = 2% to 10%. As corroborated by Figs S8–S10, the catalyst with mass ratio of 5% owns the lowest overpotentials at the same current densities, the smallest Tafel slopes and charge transfer resistance, and the largest ECSA among the three samples.

To investigate the overall water splitting performance of SA-Ru/Co(OH)F under practical application conditions, an electrolyzer was assembled using the SA-Ru/Co(OH)F as the anode and commercial Pt/C as the cathode for catalyzing the overall water splitting in 1.0 mol L^{-1} KOH electrolyte. The overall water splitting performance of a RuO_2||Pt/C system was also recorded for reference. Fig. 4a shows the polarization curve of SA-Ru/Co(OH)F||Pt/C, which delivers a current density of 10 mA cm^{-2} at a voltage of 1.56 V, about 80 mV lower than that of the RuO_2||Pt/C cell to output the same current density. This result demonstrates the SA-Ru/Co(OH)F is an excellent electrocatalyst, suitable for employing as anode of alkaline electrolyzer for water splitting. Besides, after more than 19 h of continuous water electrolysis at a fixed voltage of 1.56 V, the current density of SA-Ru/Co(OH)F||Pt/C maintains around 10 mA cm^{-2}. This evidences that the SA-Ru/Co(OH)F owns a superior durability under practical application conditions.

Overall, the prominently enhanced electrocatalytic performance of SA-Ru/Co(OH)F nanoarrays are ascribed to the advanced structure with numerous superiorities: (i) The electronic structure of single-atom Ru can be tuned *via* the strong electronic coupling with Co(OH)F, leading to the improved intrinsic catalytic activity. Meanwhile, the Ru single atoms can be stabilized by Co(OH)F by preventing the further oxidation to RuO_4^{2-}, and thus

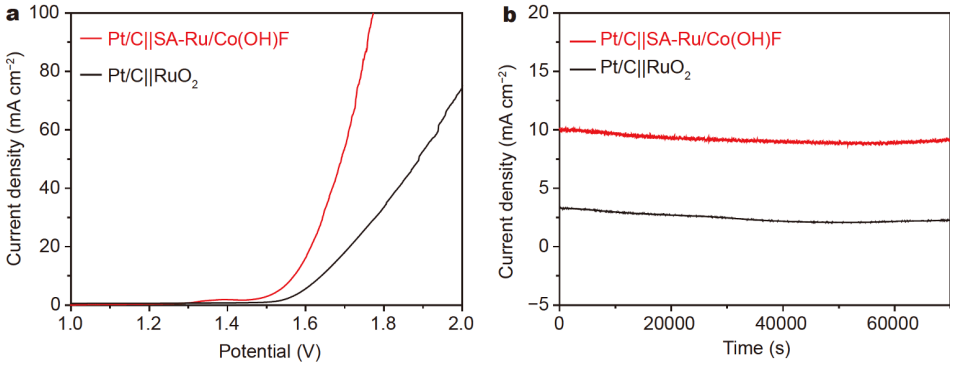

Figure 4 Catalytic performance in overall water splitting devices: (a) polarization curves of Pt/C||SA-Ru/Co(OH)F and Pt/C||RuO_2; (b) durability test at a constant potential of 1.56 V for 70,000 s.

avoids the dissolution problem [17]. (ii) The nanosheet morphology of SA-Ru/Co(OH)F benefits the well dispersion of Ru on the Co(OH)F substrate, exposing more active sties and increasing the contact area between the electrode material and the electrolyte [9]. (iii) 3D hierarchical nanoarrays endow the SA-Ru/Co(OH)F catalyst with high mechanical stability [31], while the sufficient space is beneficial for mass transfer and gas bubbles. In addition, the fabrication of SA-Ru/Co(OH)F catalyst is energy-efficient and easily scalable. Accordingly, the above mentioned advantages make the SA-Ru/ Co(OH)F a promising and competitive electrocatalyst for catalyzing the oxygen evolution in industrial alkaline electrolysis of water.

CONCLUSIONS

In summary, atomically dispersed Ru on 3D Co(OH)F nanosheet arrays was fabricated by a mild hydrothermal reaction. With 0.5 wt% Ru loading, the resultant Ru/Co(OH)F catalyst displayed outstanding activity and excellent stability toward OER in alkaline medium. An overpotential of 326 mV is needed to achieve a large current density of 500 mA cm^{-2}, much better than those of the state-of-the-art RuO_2 and most of the recently reported catalysts. The anchoring of Ru on the Co(OH)F nanoarrays can enhance the intrinsic activity as well as electrochemical and structural stabilities by the strong electronic coupling. The interlaced 3D nanosheet array architecture further contributes to the improved catalytic performance. When used as the anode of an overall water splitting device, the SA-Ru/Co(OH)F catalyst also exhibited satisfactory OER activity and stability. This work emphasizes that ultra-low content Ru can be used to modify non-noble metal-based OER electrocatalysts in order to enhance the current densities for industrial water electrolysis.

Received 8 September 2020; accepted 30 September 2020; published online 28 December 2020

1 Chu S, Majumdar A. Opportunities and challenges for a sustainable energy future. Nature, 2012, 488: 294–303
2 Hosseini SE, Wahid MA. Hydrogen production from renewable and sustainable energy resources: Promising green energy carrier for clean development. Renew Sustain Energy Rev, 2016, 57: 850–866
3 Suntivich J, May KJ, Gasteiger HA, *et al.* A perovskite oxide optimized for oxygen evolution catalysis from molecular orbital principles. Science, 2011, 334: 1383–1385
4 Wang Q, Huang X, Zhao ZL, *et al.* Ultrahigh-loading of Ir single atoms on NiO matrix to dramatically enhance oxygen evolution reaction. J Am Chem Soc, 2020, 142: 7425–7433
5 Zhang H, Tian W, Duan X, *et al.* Catalysis of a single transition metal site for water oxidation: From mononuclear molecules to single atoms. Adv Mater, 2020, 32: 1904037
6 Qin Q, Jang H, Chen L, *et al.* Low loading of Rh_xP and RuP on N, P codoped carbon as two trifunctional electrocatalysts for the oxygen and hydrogen electrode reactions. Adv Energy Mater, 2018, 8: 1801478
7 Katsounaros I, Cherevko S, Zeradjanin AR, *et al.* Oxygen electrochemistry as a cornerstone for sustainable energy conversion. Angew Chem Int Ed, 2014, 53: 102–121
8 Zhuang L, Jia Y, Liu H, *et al.* Sulfur-modified oxygen vacancies in iron-cobalt oxide nanosheets: Enabling extremely high activity of the oxygen evolution reaction to achieve the industrial water splitting benchmark. Angew Chem Int Ed, 2020, 59: 14664–14670
9 Qin Q, Jang H, Li P, *et al.* A tannic acid-derived N-, P-codoped carbon-supported iron-based nanocomposite as an advanced trifunctional electrocatalyst for the overall water splitting cells and zinc-air batteries. Adv Energy Mater, 2019, 9: 1803312
10 Cherevko S, Geiger S, Kasian O, *et al.* Oxygen and hydrogen evolution reactions on Ru, RuO_2, Ir, and IrO_2 thin film electrodes in acidic and alkaline electrolytes: A comparative study on activity and stability. Catal Today, 2016, 262: 170–180
11 Dong C, Zhang X, Xu J, *et al.* Ruthenium-doped cobalt-chromium layered double hydroxides for enhancing oxygen evolution

through regulating charge transfer. Small, 2020, 16: 1905328
12 Bai L, Duan Z, Wen X, *et al.* Highly dispersed ruthenium-based multifunctional electrocatalyst. ACS Catal, 2019, 9: 9897–9904
13 Zhou KL, Wang C, Wang Z, *et al.* Seamlessly conductive $Co(OH)_2$ tailored atomically dispersed Pt electrocatalyst with a hierarchical nanostructure for an efficient hydrogen evolution reaction. Energy Environ Sci, 2020, 13: 3082–3092
14 Shan J, Li M, Allard LF, *et al.* Mild oxidation of methane to methanol or acetic acid on supported isolated rhodium catalysts. Nature, 2017, 551: 605–608
15 Yang XF, Wang A, Qiao B, *et al.* Single-atom catalysts: A new frontier in heterogeneous catalysis. Acc Chem Res, 2013, 46: 1740–1748
16 Li X, Bi W, Zhang L, *et al.* Single-atom Pt as Co-catalyst for enhanced photocatalytic H_2 evolution. Adv Mater, 2016, 28: 2427–2431
17 Li P, Wang M, Duan X, *et al.* Boosting oxygen evolution of single-atomic ruthenium through electronic coupling with cobalt-iron layered double hydroxides. Nat Commun, 2019, 10: 1711
18 Fei H, Dong J, Feng Y, *et al.* General synthesis and definitive structural identification of MN_4C_4 single-atom catalysts with tunable electrocatalytic activities. Nat Catal, 2018, 1: 63–72
19 Cui X, Li W, Ryabchuk P, *et al.* Bridging homogeneous and heterogeneous catalysis by heterogeneous single-metal-site catalysts. Nat Catal, 2018, 1: 385–397
20 Fu Z, Ling C, Wang J. A $Ti_3C_2O_2$ supported single atom, trifunctional catalyst for electrochemical reactions. J Mater Chem A, 2020, 8: 7801–7807
21 Tong Y, Chen P, Zhou T, *et al.* A bifunctional hybrid electrocatalyst for oxygen reduction and evolution: Cobalt oxide nanoparticles strongly coupled to B,N-decorated graphene. Angew Chem Int Ed, 2017, 56: 7121–7125
22 Ben Yahia H, Shikano M, Tabuchi M, *et al.* Synthesis and characterization of the crystal and magnetic structures and properties of the hydroxyfluorides Fe(OH)F and Co(OH)F. Inorg Chem, 2014, 53: 365–374
23 Wan S, Qi J, Zhang W, *et al.* Hierarchical Co(OH)F superstructure built by low-dimensional substructures for electrocatalytic water oxidation. Adv Mater, 2017, 29: 1700286
24 Lv J, Yang X, Zang HY, *et al.* Ultralong needle-like N-doped Co(OH)F on carbon fiber paper with abundant oxygen vacancies as an efficient oxygen evolution reaction catalyst. Mater Chem Front, 2018, 2: 2045–2053
25 Liu Y, Liang X, Gu L, *et al.* Corrosion engineering towards efficient oxygen evolution electrodes with stable catalytic activity for over 6000 hours. Nat Commun, 2018, 9: 2609
26 Yang Y, Fei H, Ruan G, *et al.* Porous cobalt-based thin film as a bifunctional catalyst for hydrogen generation and oxygen generation. Adv Mater, 2015, 27: 3175–3180
27 Liao L, Wang S, Xiao J, *et al.* A nanoporous molybdenum carbide nanowire as an electrocatalyst for hydrogen evolution reaction. Energy Environ Sci, 2014, 7: 387–392
28 Liu D, Li X, Chen S, *et al.* Atomically dispersed platinum supported on curved carbon supports for efficient electrocatalytic hydrogen evolution. Nat Energy, 2019, 4: 512–518
29 Zhang G, Wang B, Li L, *et al.* Phosphorus and yttrium codoped Co(OH)F nanoarray as highly efficient and bifunctional electrocatalysts for overall water splitting. Small, 2019, 15: 1904105
30 Xiong Y, Xu L, Jin C, *et al.* Interface-engineered atomically thin Ni_3S_2/MnO_2 heterogeneous nanoarrays for efficient overall water splitting in alkaline media. Appl Catal B-Environ, 2019, 254: 329–338
31 Cui Y, Zhang J, Jin C, *et al.* Ionic liquid-controlled growth of $NiCo_2S_4$ 3D hierarchical hollow nanoarrow arrays on Ni foam for superior performance binder free hybrid supercapacitors. Small, 2018, 15: 1804318
32 Liang G, Zhou Y, Zhao J, *et al.* Structure-sensitive and insensitive reactions in alcohol amination over nonsupported Ru nanoparticles. ACS Catal, 2018, 8: 11226–11234
33 Yao Q, Huang B, Zhang N, *et al.* Channel-rich RuCu nanosheets for pH-universal overall water splitting electrocatalysis. Angew Chem Int Ed, 2019, 58: 13983–13988
34 Yang K, Xu P, Lin Z, *et al.* Ultrasmall Ru/Cu-doped RuO_2 complex embedded in amorphous carbon skeleton as highly active bifunctional electrocatalysts for overall water splitting. Small, 2018, 14: 1803009
35 Gordy W, Oriville Thomas WJ. Electronegativities of the elements. J Chem Phys, 1956, 24: 439–444
36 Kuo DY, Paik H, Kloppenburg J, *et al.* Measurements of oxygen electroadsorption energies and oxygen evolution reaction on RuO_2 (110): A discussion of the sabatier principle and its role in electrocatalysis. J Am Chem Soc, 2018, 140: 17597–17605
37 Yang J, Liu H, Martens WN, *et al.* Synthesis and characterization of cobalt hydroxide, cobalt oxyhydroxide, and cobalt oxide nanodiscs. J Phys Chem C, 2010, 114: 111–119
38 Bajdich M, García-Mota M, Vojvodic A, *et al.* Theoretical investigation of the activity of cobalt oxides for the electrochemical oxidation of water. J Am Chem Soc, 2013, 135: 13521–13530
39 Peng Y, Zhou HY, Wang ZH. Synthesis, characterization and photocatalytic activity of Zn(OH)F hierarchical nanofibers prepared by a simple solution-based method. CrystEngComm, 2012, 14: 2812–2816
40 Chen M, Wu Y, Han Y, *et al.* An iron-based film for highly efficient electrocatalytic oxygen evolution from neutral aqueous solution. ACS Appl Mater Interfaces, 2015, 7: 21852–21859
41 Yuan S, Pu Z, Zhou H, *et al.* A universal synthesis strategy for single atom dispersed cobalt/metal clusters heterostructure boosting hydrogen evolution catalysis at all pH values. Nano Energy, 2019, 59: 472–480
42 Peng X, Zhao S, Mi Y, *et al.* Trifunctional single-atomic Ru sites enable efficient overall water splitting and oxygen reduction in acidic media. Small, 2020, 16: 2002888
43 Liu H, Yang L, Qiao K, *et al.* A new concept analogous to homogeneous catalysis to construct *in-situ* regenerative electrodes for long-term oxygen evolution reaction. Nano Energy, 2020, 76: 105115
44 Zhang Y, Wu C, Jiang H, *et al.* Atomic iridium incorporated in cobalt hydroxide for efficient oxygen evolution catalysis in neutral electrolyte. Adv Mater, 2018, 30: 1707522
45 Zhang S, Zhan G, Wang X, *et al.* Well-defined Co-Pt-OH as "electronic pump" on Co-LDH nanocages for enhanced oxygen evolution reaction. Appl Catal B-Environ, 2020, 269: 118782
46 Liu H, Sun M, Li Y, *et al.* Nanomagnetism variation with fluorine content in Co(OH)F. J Alloys Compd, 2020, 825: 153916
47 Faber MS, Dziedzic R, Lukowski MA, *et al.* High-performance electrocatalysis using metallic cobalt pyrite (CoS_2) micro- and nanostructures. J Am Chem Soc, 2014, 136: 10053–10061
48 Wang C, Qi L. Heterostructured inter-doped ruthenium-cobalt oxide hollow nanosheet arrays for highly efficient overall water splitting. Angew Chem Int Ed, 2020, 59: 17219–17224

49 Wang L, Zhou Q, Pu Z, *et al.* Surface reconstruction engineering of cobalt phosphides by Ru inducement to form hollow Ru-RuP_x-Co_xP pre-electrocatalysts with accelerated oxygen evolution reaction. Nano Energy, 2018, 53: 270–276

50 Qin Q, Chen L, Wei T, *et al.* MoS_2/NiS yolk-shell microsphere-based electrodes for overall water splitting and asymmetric supercapacitor. Small, 2019, 15: 1803639

51 Han M, Wang N, Zhang B, *et al.* High-valent nickel promoted by atomically embedded copper for efficient water oxidation. ACS Catal, 2020, 10: 9725–9734

Acknowledgements This work was supported by Taishan Scholar Program of Shandong Province, China (ts201712045), Shandong Provincial Key Research and Development Program (2019GGX102069), the Natural Science Foundation of Shandong Province of China (ZR2018BB008), Doctoral Found of Qingdao University of Science and Technology (0100229001 and 010029081) and 2019 Research Funds of Ulsan National Institute of Science and Technology, South Korea (1.190002.01).

Author contributions Liu X and Cho J proposed the research and designed the experiments; Qin Q and Liu X performed the analysis and wrote the manuscript; Zhou S, Li Z and Li C conducted material synthesis and electrochemical measurements; Jang H and Kim MG conducted XAS and other physical characterizations. All authors discussed the results and commented on the manuscript.

Conflict of interest The authors declare that they have no conflict of interest.

Supplementary information Experimental details and supporting data are available in the online version of the paper.

Shizheng Zhou is currently pursuing his PhD degree under the supervision of Prof. Xien Liu at Qingdao University of Science and Technology. His current research interests focus on the design and syntheses of noble metal-based electrocatalysts for HER and OER.

Qing Qin received her PhD degree in 2017 from Nankai University. Now she is a professor of Qingdao University of Science and Technology. Her current research interests focus on the design and syntheses of noble metal- and non-noble metal-based electrocatalysts for overall water splitting and Zn-air batteries.

Xien Liu received his PhD degree from Dalian University of Technology. He is currently a professor of Qingdao University of Science and Technology. His research interests focus on the design of electrocatalysts for electrochemical energy conversion and storage devices.

Jaephil Cho is a professor and head of the School of Energy and Chemical Engineering at UNIST (Korea). He is a director of the Green Energy Materials Developed Center (granted by the Ministry of Trade, Industry, and Energy, South Korea) and Samsung SDI-UNIST Future Battery Research Center. His current research mainly focuses on Li-ion and metal-air batteries and redox flow batteries for energy storage.

单原子Ru修饰的三维多级Co(OH)F纳米片阵列高效催化析氧反应

周士正[1†], Haeseong Jang[2†], 秦清[1*], 李子健[3], Min Gyu Kim[4], 李创[1], 刘希恩[1*], Jaephil Cho[2*]

摘要 单原子与基底之间的电子耦合在提升单原子催化剂的本征催化活性方面起到至关重要的作用. 本文通过一步水热法在温和条件下制备了单原子Ru修饰的三维多级Co(OH)F纳米片阵列催化剂. 该催化剂在1 mol L^{-1} KOH电解液中展现出高的电催化析氧反应活性和稳定性, 在10和500 mA cm^{-2}的电流密度下分别表现出200和326 mV的过电位. 通过对催化剂析氧反应前后的电子结构和表面化学态的研究发现, 单原子Ru和Co(OH)F之间强烈的电子耦合诱导体系电荷重新分布, 并抑制了Ru在高的OER电势下被过度氧化为过高的价态(大于+4价). 本工作提供了一个通过羟基氟化钴稳定单原子Ru, 以提高大电流下析氧反应的活性和稳定性的策略.

